



HAL
open science

An integrative model of plant gravitropism linking statoliths position and auxin transport

Nicolas Levernier, Olivier Pouliquen, Yoel Forterre

► To cite this version:

Nicolas Levernier, Olivier Pouliquen, Yoel Forterre. An integrative model of plant gravitropism linking statoliths position and auxin transport. 2021. hal-03089808v2

HAL Id: hal-03089808

<https://hal.science/hal-03089808v2>

Preprint submitted on 4 Jan 2021 (v2), last revised 21 Nov 2021 (v4)

HAL is a multi-disciplinary open access archive for the deposit and dissemination of scientific research documents, whether they are published or not. The documents may come from teaching and research institutions in France or abroad, or from public or private research centers.

L'archive ouverte pluridisciplinaire **HAL**, est destinée au dépôt et à la diffusion de documents scientifiques de niveau recherche, publiés ou non, émanant des établissements d'enseignement et de recherche français ou étrangers, des laboratoires publics ou privés.

An integrative model of plant gravitropism linking statoliths position and auxin transport

Nicolas Levernier^{1,*}, Olivier Pouliquen¹ and Yoël Forterre¹

¹Aix Marseille Univ, CNRS, IUSTI, Marseille, France

Correspondence*:

IUSTI, 5 rue Enrico Fermi, 13453 Marseille cedex 13, France
nicolas.levernier@univ-amu.fr

2 ABSTRACT

3 Gravity is a major cue for proper plant growth. The response to this cue implies starch-filled
4 plastids, the statoliths, sedimenting on the bottom of statocytes cells. These statoliths are
5 assumed to modify the transport of the growth hormone by acting on specific hormone carriers,
6 PIN proteins, in an unknown way. Recent experiments show that statholiths do not act as
7 gravitational force sensor, but as position sensor. Moreover, the signal is not immediate but
8 integrated over a time-scale of a tens of minutes. However, the precise gravitropic signaling
9 pathway from the sensing of this cue at the cell scale to the response in growth at the tissue
10 scale is still not understood. Here we present a bottom-up theory that enables to rationalize the
11 previous phenomenological results from microscopic considerations. Our approach, consistent
12 with existing experimental results, tends to support that the integration time-scale is associated to
13 PIN turnover. Moreover, it leads to a revision of the so-called sine-law of plant gravitropism.

14 **Keywords:** Plant tropism, gravity sensing, integrative modeling, Auxin signaling, PIN trafficking

1 INTRODUCTION

15 The detection of gravity by plants and the resulting growth response (gravitropism) offer a fascinating
16 illustration of a multi-scale perception mechanism in living organisms (Fig. 1) (Mouliia and Fournier,
17 2009; Morita, 2010; Toyota and Gilroy, 2013). It originates in specific cells, called statocytes, where tiny
18 starch-accumulating amyloplasts acting as statoliths sediment under gravity at the bottom of the cells (Fig.
19 1 c). When the plant is inclined, the repositioning of statoliths under gravity induces a relocation of
20 auxin transporters (PIN proteins) at the membrane of statocytes, which generates a lateral transport of
21 auxin toward the lower side of the shoot or the root (Cholodni–Went hypothesis) (Fig. 1 b). In turn, this
22 asymmetry in auxin concentration induces a differential growth across the plant organ, and thus its bending
23 toward the gravity vector (Fig. 1 a). Since the pioneering works of Darwin, progress has been made on
24 every step of this gravitropic signaling pathway; yet important questions remain (Nakamura et al., 2019).
25 In particular, it is still not clear how the first physical signal generated by the sedimentation of statoliths is
26 converted into biochemical signals downstream, to eventually produce the growth response at the plant
27 scale.

28 Recently, insights into the sensing mechanism and the transduction pathway have been obtained from
29 experiments both at the macroscopic and microscopic level. First, the gravitropic response to permanent
30 stimuli (inclination of the plant), the so-called sine-law of gravitropism (Sachs, 1887; Larsen, 1969; Iino
31 et al., 1996; Galland, 2002; Dumais, 2013), was found to depend on the inclination but, surprisingly,

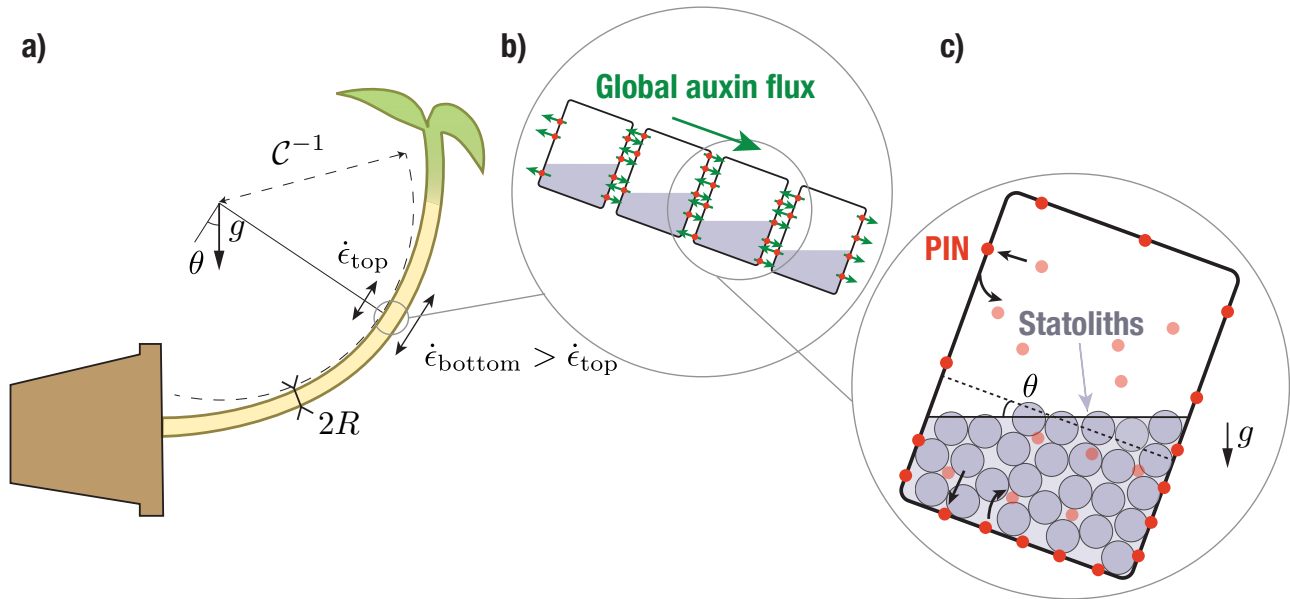


Figure 1. Multiscale description of gravitropism. At the macroscopic scale (a), the response to gravity of a shoot or a stem is achieved by differential growth across the organ, which induces a curvature of the organ. At the tissue scale (b), differential growth results from a net flux of the auxin (the growth hormone) across the width, owing to the asymmetric distribution of auxin transporters (PINs, red circles). At the cell scale (c), PIN asymmetry results from the asymmetric distribution of the statoliths position after sedimentation under gravity, which modifies PIN trafficking close to the cell membrane.

32 not on the intensity of gravity (Chauvet et al., 2016). Hence, statocytes behave like inclination sensors
 33 not force sensors as previously believed. An important consequence is that the initial gravity stimulus
 34 for gravitropism should be the position of the statoliths within statocytes (Pouliquen et al., 2017). This
 35 position-sensor hypothesis found mechanistic support from the direct observation of statoliths motion
 36 under gravity stimulation (Bérut et al., 2018). Unlike a pile of macroscopic grains like sand, statoliths were
 37 found to move and flow at any cell angle. This liquid-like behavior comes from the random agitation of the
 38 statoliths, whose origin is not thermal but arises from the interaction of statoliths with the acto-myosin
 39 cytoskeleton (Sack et al., 1986; Saito et al., 2005; Nakamura et al., 2011). A second observation came
 40 from dose-response like experiments on wheat coleoptiles in which the gravity stimulus is applied during a
 41 transient period only (Chauvet et al., 2019). When the shoots were inclined for short period of time, the
 42 gravitropic response was found to deviate from the steady response and strongly decay. The transition
 43 occurred for a time $\tau_{\text{memory}} \sim 15$ min, which was independent of gravity and much larger than the
 44 statoliths sedimentation time. This observation suggested the existence of a memory-integration process in
 45 the gravitropic signaling pathway, independent of the statoliths dynamics, that integrates the initial signal
 46 induced by statoliths displacement.

47 To account for these observations (position-sensor hypothesis, memory time independent of g), Chauvet
 48 et al. (2019) built a mathematical model of gravitropism in which the gravitropic signal controlling the
 49 differential growth was linked to the statoliths position by an integrative process of timescale τ_{memory} (a
 50 similar approach was used in Meroz et al. (2019)). Once coupled to the statoliths dynamics and the tropic
 51 growth motion, the model was able to reproduce the transient gravitropic response observed experimentally.
 52 However, Chauvet et al. (2019)'s model was built on two *ad-hoc* postulates. First, it assumes that the
 53 relation between the gravitropic signal and the statoliths position is known and given by the sine-law.

54 Second, it postulates the existence of the integrative process and time scale τ_{memory} , without explaining its
 55 origin. To go further, one has to take into account the spatio-temporal dynamics of the molecular processes
 56 acting between the statoliths and the growth response, such as the dynamics of PIN and auxin transport.

57 The objective of this paper is to fill this gap by building an integrative model of plant gravitropism that
 58 bridges the different scales of the process: (i) the initial intracellular gravitropic signal encoded in the
 59 statoliths position, (ii) PIN dynamics at the cellular level, (ii) auxin transport at the tissue level and finally
 60 (iv) differential growth and curvature at the plant organ scale. Previous models of plant gravitropism mainly
 61 focused either on the macroscopic scale, describing how the complex spatio-temporal evolution of the organ
 62 shape results from the interplay between differential growth and the slender geometry of the organ (Bastien
 63 et al., 2013, 2014; Chelakkot and Mahadevan, 2017), or on the tissue level, modeling growth mechanics
 64 (Dyson et al., 2014) or auxin transport (Band et al., 2012; Fendrych et al., 2018; Retzer et al., 2019) in
 65 realistic 1D or 3D tissue geometries. In these latter models, the distribution of PINs in the statocytes in
 66 response to plant inclination was postulated and no link was made with the intracellular dynamics of the
 67 statoliths. This is precisely the goal of this study. Building on the recent position-sensor hypothesis, we
 68 propose a simple but generic model of interaction between statoliths position and PIN recycling, that we
 69 couple with the classical equation of auxin transport and tissue growth. We will then study the gravitropic
 70 response predicted by the model for steady and unsteady gravity stimuli, comparing the results with the
 71 experimental of Chauvet et al. (2016) and Chauvet et al. (2019).

2 MATERIAL AND METHODS

72 2.1 Link between gravitropic curvature, differential growth and auxin concentration 73 gradient

74 At the plant scale, the gravitropic response is characterized by the curvature of the organ resulting from
 75 differential growth, which itself results from auxin gradients (Cholodny–Went hypothesis). The first step
 76 of the model is thus to relate those three quantities. For a slender organ like a shoot or a stem, the rate of
 77 change of the local curvature \mathcal{C} is related to differential growth through the following kinematic relationship:
 78 $R \frac{d\mathcal{C}}{dt} = \frac{1}{\tau_g} \times \frac{\dot{\epsilon}_{\text{bottom}} - \dot{\epsilon}_{\text{top}}}{2\dot{\epsilon}_{\text{mean}}}$, where R is the radius of the organ, $\dot{\epsilon}_{\text{bottom}} - \dot{\epsilon}_{\text{top}}$ is the difference of growth rate
 79 between both sides, $\dot{\epsilon}_{\text{mean}}$ is the mean growth rate and $\tau_g = \dot{\epsilon}_{\text{mean}}^{-1}$ is the growth timescale Silk (1984);
 80 Moulia and Fournier (2009) (Fig. 1). The growth rate of plant cells is known to be controlled by auxin, the
 81 so-called growth hormone. Auxin stimulates cell elongation by loosening cell walls. To the best of our
 82 knowledge, the link between the local auxin concentration in walls and the local growth rate of cells has
 83 not been robustly determined and only the response of the whole tissue to an external addition of auxin
 84 from the medium has been investigated. It is however often assumed that growth is mainly controlled
 85 by the auxin concentration in the vicinity of the ‘skin’, as epidermal tissues are stiffer than inner tissues
 86 (Kutschera and Niklas, 2007; Dyson et al., 2014). For the sake of simplicity, we will here assume that
 87 the local growth rate is simply proportional to the local auxin concentration c , $\dot{\epsilon} = kc$ Galston and Hand
 88 (1949); Hopkins and Hüner (2009), such that:

$$R \frac{d\mathcal{C}}{dt} = \frac{1}{\tau_g} \times \frac{c_{\text{bottom}} - c_{\text{top}}}{2c_{\text{mean}}}, \quad (1)$$

89 where c_{bottom} and c_{top} are the auxin concentrations on both sides of the organ and c_{mean} the mean auxin
 90 concentration. Under this assumption, the dimensionless gravitropic response deduced from the curvature
 91 dynamics, $\tilde{\Delta} \equiv R\tau_g \frac{d\mathcal{C}}{dt}$, is equal to the relative auxin gradient across the organ, $\tilde{\Delta} = \frac{c_{\text{bottom}} - c_{\text{top}}}{2c_{\text{mean}}}$. The goal
 92 of the model is to predict how this auxin gradient establishes when the plant is tilted.

93 2.2 Auxin transport

94 Auxin transport plays a key role in shaping plants development and, as such, has been the topic of
 95 extensive research over the past decades. Auxin transport is based on two distinct mechanisms (Goldsmith,
 96 1977; Hopkins and Hüner, 2009; Runions et al., 2014). On the one hand, auxin in cell walls (mostly in a
 97 protonated form) enters the neighboring cell passively, or thanks to Aux/Lax influx carriers that are evenly
 98 distributed throughout the membrane. On the other hand, auxin inside cells (mostly in an anionic form)
 99 can only exit thanks to active auxin efflux carriers, such as PIN proteins (Krecek et al., 2009) or ABCB
 100 transporters (Zažímalová et al., 2010). While ABCB are evenly distributed throughout the membrane, PIN
 101 proteins are usually polarized and can be redistributed in response to external stimuli such as gravity (in
 102 particular PIN3, which is known to be implied in gravitropic response, Friml et al. (2002)). Hence, an
 103 asymmetric distribution of PIN carriers on each side of the cell can generate an active transport of auxin
 104 from one cell to the other, resulting in a stable auxin gradient.

To model this situation, we provide a simplified description of auxin transport in which the different forms of auxin (proton-associated or not) are not taken into account. The tissue across the shoot or stem (width $2R$) is modeled as a one-dimensional array of N cells of width W separated by a cell wall of width w (Fig. 1 and Fig. 2). We denote c_n the auxin concentration inside the n -th cell and C_n the auxin concentration inside the n -th wall, which are both assumed uniform (the equilibrium time of auxin in each compartment is very fast, about 0.1 s in the cell wall and few s inside the cell taking typical values of auxin diffusion coefficients, Kramer et al. (2007)). We also neglect auxin dilution due to cell growth and assume that auxin is neither degraded nor created, as the degradation time of auxin (of the order of the day, Grieneisen et al. (2012)) is much longer than the minutes to hours timescales we are interested in. The efflux current of auxin (number of auxin molecules per unit time and unit surface) from the n -th cell to the left wall (resp. right wall) is given by $P_n^l c_n$ (resp. $P_n^r c_n$), where P_n^l (resp. P_n^r) is the permeability of the left (resp. right) membrane (unit m/s). Conversely, the influx current of auxin from the n -th wall to both

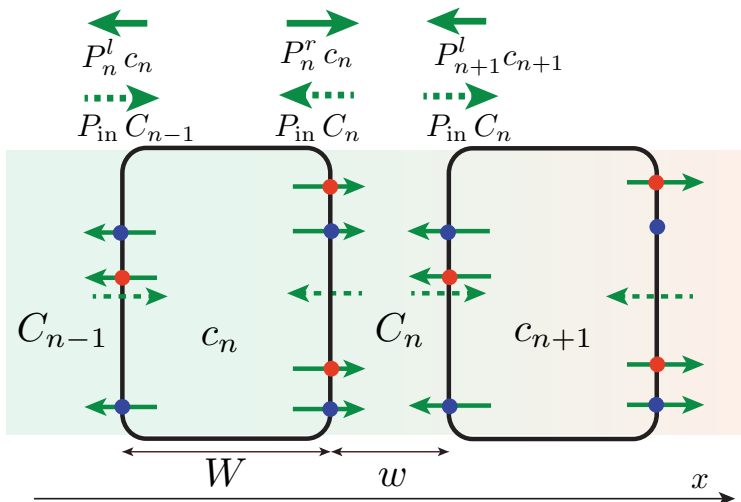


Figure 2. One-dimensional, discrete model of auxin transport across the tissue (in reality $w \ll W$). Efflux of auxin (solid green arrow) occurs through efflux carriers (PIN: red circle, ABCB: blue circle), whose distribution (and thus permeabilities $P_n^{l,r}$) can be different on the right and left membrane of the cell. By contrast, influx of auxin (green dotted arrow) occurs with a symmetrical permeability P^{in} on both side of the cell. An asymmetry of efflux permeabilities $P^l \neq P^r$ can generate a net flux of auxin across the tissue, yielding an auxin concentration gradient (background color gradient).

adjacent cells is $P^{\text{in}}C_n$, where the influx permeability P^{in} is assumed uniform for all cells (see Fig. 2). The time-evolution of the concentration is then:

$$w \frac{dC_n}{dt} = -2P^{\text{in}}C_n + P_n^r c_n + P_{n+1}^l c_{n+1}, \tag{2}$$

$$W \frac{dc_n}{dt} = -(P_n^l + P_n^r)c_n + P^{\text{in}}(C_{n-1} + C_n). \tag{3}$$

105 The cell wall size being much smaller than the cell width ($w \ll W$), the auxin concentration in the cell
 106 wall can be assumed quasi-steady, $2P^{\text{in}}C_n \simeq P_n^r c_n + P_{n+1}^l c_{n+1}$, yielding:

$$2W \frac{dc_n}{dt} = P_{n+1}^l c_{n+1} - P_n^l c_n + P_{n-1}^r c_{n-1} - P_n^r c_n. \tag{4}$$

107 In the following, we assume that the distribution of auxin efflux carriers is the same in each cell, so that P^l
 108 and P^r are independent of n . This is the case of shoot coleoptiles where all cells in the growing region
 109 are similar and contain statoliths, but not the case of many stems like Arabidopsis inflorescence where
 110 statoliths are only present on an external ring in the endodermal cells (the modification of the equation in
 111 this case of inhomogeneous tissue is given in Appendix A). We also assume that auxin gradients occur over
 112 a length scale much larger than the cell size. In the continuum limit [$c_n(t) \rightarrow c(x, t)$], equation 4 for auxin
 113 transport then reduces to an advection-diffusion equation given by:

$$\frac{\partial c}{\partial t} = \mathcal{D} \frac{\partial^2 c}{\partial x^2} - v \frac{\partial c}{\partial x} \tag{5}$$

114 where $\mathcal{D} = WP/2$ is the coefficient of diffusion and $v = \delta P/2$ the advection speed, with $P = (P^l + P^r)/2$
 115 and $\delta P = P^r - P^l$.

116 The advective part of the equation (5), which is responsible for auxin transport from one side to the other
 117 and eventually to differentiated growth and curvature of the organ, is entirely controlled by the asymmetry
 118 of efflux permeabilities δP . Since ABCB carriers are evenly distributed, this asymmetry comes from the
 119 asymmetry of PIN distribution between the right and left side of the cells:

$$\delta P = P^r - P^l = \frac{1}{S} \left(\alpha \int_S [PIN]_{|\text{right}} - \alpha \int_S [PIN]_{|\text{left}} \right), \tag{6}$$

120 where α is the conductance of a single PIN carrier (unit m^3/s), S the lateral surface of the cells and
 121 $[PIN]$ the surface concentration of PIN attached to the membrane. In the following, we assume that the
 122 efflux permeability due to ABCB carriers is much larger than the efflux permeability due to PIN, such
 123 that $P = (P^l + P^r)/2 \simeq (1/S)\beta \int [ABCB]$, where β is the conductance of a single ABCB carrier, is
 124 independent of PIN concentration. This enables us to take a constant coefficient of diffusion \mathcal{D} in the
 125 model, which simplifies the results without affecting much the conclusions.

126
 127 **2.3 Coupling PIN dynamics to statoliths position: biased efflux at cell scale**

128 The previous section relates auxin transport to the asymmetry of PINs distribution at the cellular level.
 129 We now model how this asymmetry emerges when the plant is tilted under gravity. Recently, it has been
 130 demonstrated that the relevant gravitropic stimulus for graviperception is the statoliths position within
 131 the statocytes (position-sensor hypothesis), and not their weight as previously believed Chauvet et al.

132 (2016); Pouliquen et al. (2017). Statoliths have also been identified as key actors in the relocalisation
 133 of PIN-proteins in response to change of gravity direction Nakamura et al. (2019). Yet, how statoliths
 134 position is detected and read to modify PIN polarity remains largely unknown. PINs trafficking involves
 135 synthesis in the endoplasmic reticulum, degradation in the vacuole and recycling Kleine-Vehn and Friml
 136 (2008). Recycling is achieved by endocytosis, i.e., the deallocation of PIN proteins formerly attached to
 137 the cell membrane toward the cytoplasm inside a vesicle, or by exocytosis, i.e., the reallocation of the
 138 vesicle-carried PINs from the cytoplasm back to the cell membrane.

139 Following the position-sensor hypothesis, we assume that the presence of statoliths, either through direct
 140 steric constraints or through indirect molecular signaling, modify the trafficking of PIN proteins, so that
 141 PINs tend to enter the cell membrane preferentially on places where statoliths are in contact with it. This
 142 mechanism is formalized as follows. The endocytosis rate of PINs, $d[PIN]_i/dt = -k_{\text{off},i}[PIN]_i$ where
 143 $[PIN]_i$ is the surface concentration of PIN attached to the membrane, is assumed to depend on the presence
 144 of statoliths, with $i = 0$ if no statoliths are present and $i = 1$ if they are (see Fig. 3). Similarly, the rate of
 145 exocytosis is written as $d[PIN]_i/dt = +k_{\text{on},i}(N_{\text{vol}}/N_{\text{tot}})$, where N_{vol} is the number of PINs molecules
 146 inside the cell and N_{tot} the total number of PINs both inside the cell and attached to the membrane. Two
 147 cases will be distinguished in the model, depending on whether PINs can attach to any side of the cell
 148 ("apical/basal/lateral binding") or only on lateral sides ("lateral binding") (see Fig. 4 a). Assuming that
 149 the total number N_{tot} of PINs is conserved during gravistimulation (Kleine-Vehn et al., 2010) leads to the
 150 following set of equations for the PIN concentration attached to the membrane, $[PIN]_{i=0,1}$:

$$\begin{aligned} \frac{d[PIN]_0}{dt} &= -k_{\text{off},0} [PIN]_0 + k_{\text{on},0} \left(1 - \frac{S_0[PIN]_0 + S_1[PIN]_1}{N_{\text{tot}}} \right) \\ \frac{d[PIN]_1}{dt} &= -k_{\text{off},1} [PIN]_1 + k_{\text{on},1} \left(1 - \frac{S_0[PIN]_0 + S_1[PIN]_1}{N_{\text{tot}}} \right) \end{aligned} \quad (7)$$

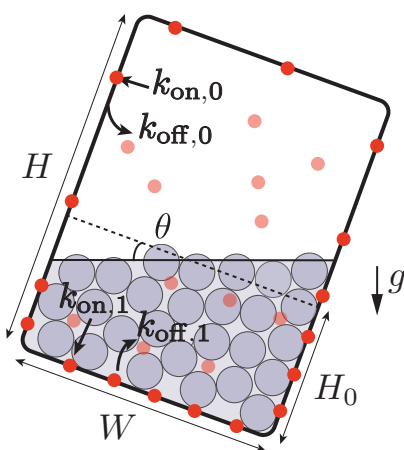


Figure 3. Interaction between PIN trafficking and statoliths position. The rate of reallocation k_{on} and deallocation k_{off} of PINs (bold red circles: PINs attached to the cell membrane, light red circles: PINs in bulk) depends on the presence of statoliths (grey). When the cell is tilted, the asymmetric distribution of the position of the statoliths induces a bias in the distribution of the PINs attached to the membrane.

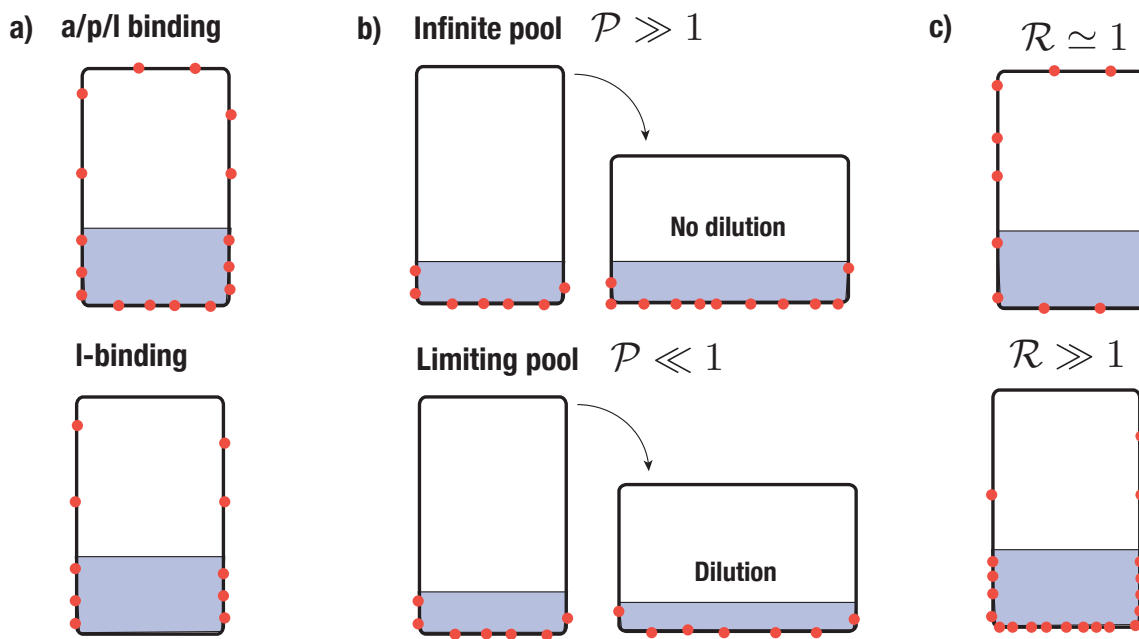


Figure 4. Sketch of different scenario of PIN-binding. PINs are represented in red and the region with statoliths in blue. (a) Apical/basal/lateral-binding vs lateral-binding. (b) Infinite pool versus limiting pool. In the first case, the density of PIN is conserved whereas in the second one, the total number of PIN is. (c) Low sensitivity of PIN to statoliths ($\mathcal{R} \simeq 1$) or high sensitivity ($\mathcal{R} \gg 1$).

151 where S_1 (resp. S_0) denotes the total surface in contact (resp. not in contact) with statoliths in case of
 152 apical/basal/lateral binding, or only the lateral surfaces in contact (resp. not in contact) with statoliths in
 153 the lateral binding case.

154 The form of equation (7) shows that two regimes can be distinguished, depending on whether N_{tot} is
 155 large or small compared to $Sk_{\text{on}}/k_{\text{off}}$. The first regime, called ‘infinite-pool’ regime in the following,
 156 corresponds to the case where $N_{\text{tot}}k_{\text{off}}/Sk_{\text{on}}$ is so large that binding is only limited by k_{off} . The second
 157 regime, called ‘limiting-pool’ regime, corresponds to the opposite situation where the total number of
 158 attached carriers is strongly limited by N_{tot} , such that $S_0[\text{PIN}]_0 + S_1[\text{PIN}]_1 \simeq N_{\text{tot}}$ (see Fig. 4 b).
 159 Finally, we note that in writing Eq. (7), we have neglected the diffusion of PINs inside the membrane.
 160 This is justified since, over the time scales we are interesting in (running from minutes to one hour), PINs
 161 diffuse only over a distance of about few micrometers, which is much smaller than the cell size (taking
 162 $0.1\mu\text{m}^2$ min for the diffusion coefficient of PIN, see Kleine-Vehn et al. (2011)).

3 RESULTS

163 3.1 Steady gravitropic response: revisited sine-law

164 We first study the gravitropic response predicted by our model in the case of a steady inclination of the
 165 plant θ , for timescales long enough that the system reaches a steady state. This situation corresponds to the
 166 usual protocol for measuring the sensitivity of plant to gravity under steady condition, when the plant is
 167 suddenly inclined to a fixed angle and its curvature (or tip angle) measured over long timescale. After a
 168 transient, the rate of change of curvature is found to be constant Chauvet et al. (2016), which enables to
 169 measure the gravitropic response $\tilde{\Delta}^{\text{steady}}(\theta) = R\tau_g \frac{dC}{dt}$ (see Material and Methods) for each imposed angle
 170 θ . For many plants, this relationship between the gravitropic response and the inclination angle has sine-like

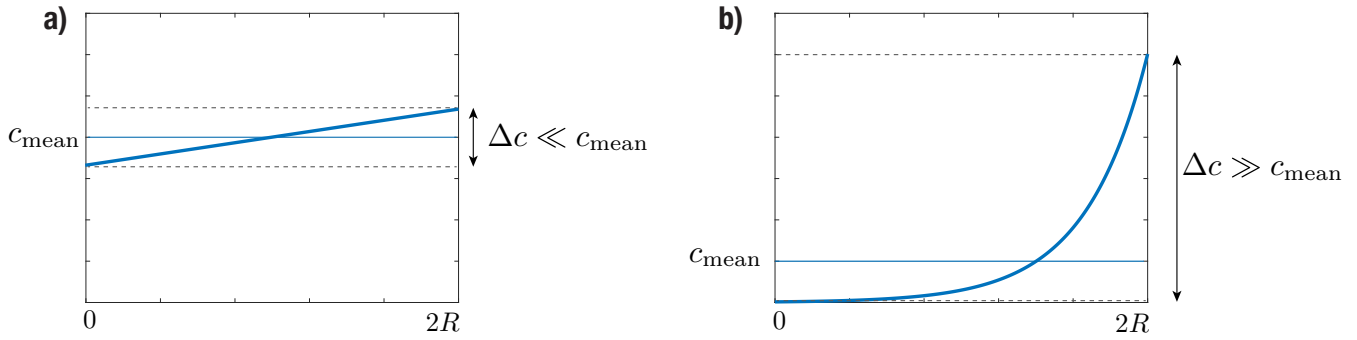


Figure 5. Stationary auxin profile for (a) small and (b) large Peclet number.

171 shape (the response is null for $\theta = 0^\circ$ or $\theta = 180^\circ$ and maximal for $\theta = 90^\circ$) and is called the ‘sine-law’ of
 172 plant gravitropism in the literature (Sachs, 1887; Larsen, 1969; Iino et al., 1996; Galland, 2002; Dumais,
 173 2013). Below, we determine the steady gravitropic response $\tilde{\Delta}^{\text{steady}}(\theta)$ predicted by the model eqs (1, 5,
 174 7) and compare with measurements of the sine-law obtained previously for wheat coleoptiles over a wide
 175 range of angles Chauvet et al. (2016).

176 In the steady regime, the auxin transport equation (5) reduces to: $dJ/dx = 0$, where $J = \mathcal{D}(dc/dx) - vc$
 177 is the auxin flux. For impermeable boundaries at $x = 0$ and $x = 2R$, the flux is null and the auxin
 178 concentration profile is given by:

$$c(x) = c_{\text{mean}} \frac{\text{Pe} \times \exp\left(\text{Pe} \frac{x}{2R}\right)}{\exp(\text{Pe}) - 1}, \quad (8)$$

179 where $c_{\text{mean}} = (1/2R) \int_0^{2R} c(x) dx$ is the mean concentration of auxin and Pe is the Peclet number given
 180 by:

$$\text{Pe} = \frac{2Rv}{\mathcal{D}} = N \frac{\delta P}{P} = N \frac{\alpha \left(\int_S [PIN]_{\text{right}} - \int_S [PIN]_{\text{left}} \right)}{\beta \int [ABC B]}. \quad (9)$$

181 For $\text{Pe} \ll 1$, the profile is linear and the auxin level in the middle of the stem is unchanged, whereas for
 182 $\text{Pe} \gg 1$ the profile is strongly asymmetric with most auxin concentrated on the right (Fig. 5). From this
 183 steady profile of auxin, the gravitropic response can be computed as $\tilde{\Delta}^{\text{steady}} = \frac{c(x=2R) - c(x=0)}{2c_{\text{mean}}}$ (eq. (1),
 184 which gives:

$$\tilde{\Delta}^{\text{steady}} = \frac{\text{Pe}}{2} \quad (10)$$

185 In the steady state, the gravitropic response of the plant is thus given by the value of the Peclet number.
 186 Previous measurements in various plant species representative of land angiosperm showed that $\tilde{\Delta}^{\text{steady}}$ is
 187 typically of the order 1 Chauvet et al. (2016) (for e.g. in wheat coleoptile, the maximal value of $\tilde{\Delta}^{\text{steady}}$
 188 obtained for a 90 degrees inclination is about 0.7), meaning that the Peclet number is typically of the
 189 order 1. Therefore, the auxin profile across the shoot is expected to be close to linear (Fig. 5 a) (and not
 190 a pronounced exponential, Fig. 5 b). A consequence is that growth, which was assumed proportional to
 191 the auxin concentration, varies also linearly from one side of the shoot to the other during the gravitropic
 192 response.

193 The next step to determine $\tilde{\Delta}^{\text{steady}}$ is to compute the Peclet number (9), i.e., the relative distribution of
 194 PIN between the left and right side of the cell. In the steady regime, the concentration of PIN attached to a
 195 membrane not covered by statoliths ($[PIN]_0$), or covered by statoliths ($[PIN]_1$), is given by (see eq. 7):

$$\begin{aligned}
 [PIN]_0 &= \left(\frac{k_{\text{off},0}}{k_{\text{on},0}} + \frac{1}{N_{\text{tot}}} \left[S_0 + \frac{k_{\text{on},1} k_{\text{off},0}}{k_{\text{on},0} k_{\text{off},1}} S_1 \right] \right)^{-1} \\
 [PIN]_1 &= \left(\frac{k_{\text{off},1}}{k_{\text{on},1}} + \frac{1}{N_{\text{tot}}} \left[S_1 + \frac{k_{\text{on},0} k_{\text{off},1}}{k_{\text{on},1} k_{\text{off},0}} S_0 \right] \right)^{-1}
 \end{aligned}
 \tag{11}$$

196 Noting S_i^l (resp. S_i^r) the surface of the left (resp. right) side of the cell not covered ($i = 0$) or covered
 197 ($i = 1$) by statoliths, we have $\int_S [PIN]_{|\text{right}} - \int_S [PIN]_{|\text{left}} = [PIN]_0(S_0^r - S_0^l) + [PIN]_1(S_1^r - S_1^l)$.
 198 Finally, since $S_0^l + S_1^r = S_0^r + S_1^l = S$, where S is the lateral surface of the cells and using (9), we have:

$$\tilde{\Delta}^{\text{steady}} = \frac{\alpha N (\mathcal{R} - 1) (S_1^r - S_1^l) [PIN]_0}{2\beta \int [ABCB]}
 \tag{12}$$

199 with

$$[PIN]_0 = \frac{k_{\text{on},1}}{k_{\text{off},1} \mathcal{R}} \left(1 + \mathcal{P}^{-1} \frac{S_1}{S} \left(1 + \frac{S_0}{S_1 \mathcal{R}} \right) \right)^{-1}
 \tag{13}$$

200 and:

$$\mathcal{R} = \frac{[PIN]_1}{[PIN]_0} = \frac{k_{\text{on},1} k_{\text{off},0}}{k_{\text{on},0} k_{\text{off},1}}, \quad \mathcal{P} = \frac{N_{\text{tot}} k_{\text{off},1}}{k_{\text{on},1} S}
 \tag{14}$$

201 The expressions (12–14) show that the steady gravitropic response is proportional to $(\mathcal{R} - 1)(S_1^r - S_1^l)$. For
 202 $\theta > 0$ as in Fig. 1, the difference $(S_1^r - S_1^l)$ is positive since statoliths sediment toward the right side of the
 203 cell. Therefore, to obtain a ‘normal’ gravitropic response ($\tilde{\Delta}^{\text{steady}} > 0$, i.e., a larger auxin concentration
 204 at the bottom side of the shoot), the ratio \mathcal{R} must be larger than 1. The parameter \mathcal{R} is the ratio between
 205 the concentration of PIN in a zone with statolith and in a zone without statolith, hence the larger \mathcal{R} , the
 206 more PIN in the region with statoliths compared to region without statolith (see Fig 4 c). The other main
 207 parameter controlling the gravitropic response is the pool number \mathcal{P} , where $\mathcal{P} \gg 1$ corresponds to the
 208 infinite-pool regime and $\mathcal{P} \ll 1$ corresponds to the limiting-pool regime (see Fig 4 b).

209 Once \mathcal{R} and \mathcal{P} are set, the final step is to compute how the different surfaces covered (and not covered)
 210 by the statoliths vary as function of the inclination angle θ . To this end, one has to know the final position
 211 of statoliths when a cell is tilted. Recently, we address this question and showed that statoliths at the bottom
 212 of statocytes behave like an effective liquid on long timescale, due to the agitation of statoliths by the cell
 213 activity Bérut et al. (2018). Therefore, the final free surface of the statoliths pile is horizontal, as sketched
 214 in Fig. 3. This key feature of the flowing behavior of statoliths allows us to reduce the computation of
 215 the surfaces in (12, 13) to a purely geometrical problem that depends on three parameters: the angle of
 216 inclination θ , the aspect ratio of the cell H/W and the initial aspect ratio of the statolith pile H_0/W (see
 217 Fig. 3). The corresponding relationships are given in Appendix B.

218 Fig. 6 presents the typical steady gravitropic response $\tilde{\Delta}^{\text{steady}}(\theta)$ predicted by the model (12, 13, 14) as
 219 a function of θ , in the case of an infinite pool ($\mathcal{P} \gg 1$) or a limiting pool ($\mathcal{P} \ll 1$), and for two extreme
 220 values of \mathcal{R} : $\mathcal{R} \simeq 1$ (red curve, low influence of statoliths on PIN binding) and $\mathcal{R} \gg 1$ (blue curve, strong
 221 influence of statoliths on PIN binding). The geometry used for the cell aspect ratio and the statoliths pile

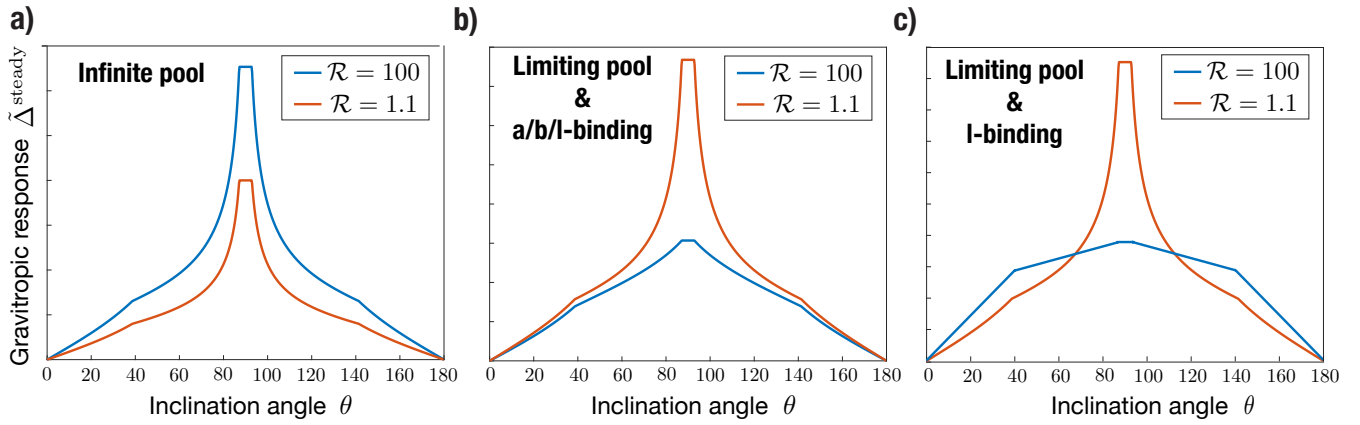


Figure 6. Steady gravitropic response $\tilde{\Delta}^{\text{steady}}$ (arbitrary amplitude) as a function of the inclination angle θ , for \mathcal{R} either large or close to 1, in the case of (a) infinite pool ($\mathcal{P} \gg 1$), (b) limiting pool ($\mathcal{P} \ll 1$) with apical/basal/lateral binding, (c) limiting pool ($\mathcal{P} \ll 1$) with lateral binding only. Note that in the case of an infinite pool, results are the same in the a/b/l-binding or l-binding case. Geometrical parameters used are $H_0 = 4d$, $W = 10d$, $H = 25d$ where d stands for the diameter of a statolith.

222 ratio is taken from experimental observations of wheat coleoptile statocytes, with a typical aspect ratio
 223 $H/W = 2.5$ and $H_0/W = 1/2.5$. In the case of an infinite pool (Fig. 6 a), the gravitropic response presents
 224 a convex shape with a strong peak close to 90° whatever the value of \mathcal{R} , in disagreement with the usual
 225 sine-law. The amplitude of this peak is related to the cell geometry: the more elongated the cell, the higher
 226 the peak; this is because more lateral surface is available for PIN attachment, without any limitation on the
 227 quantity of PIN in the infinite-pool regime (no dilution, see Fig 4 b). By contrast, in the limiting-pool case
 228 (Fig. 6 b,c), the response strongly depends on \mathcal{R} , the peak at 90° being much smaller for $\mathcal{R} \gg 1$ than for
 229 $\mathcal{R} \simeq 1$. Interestingly, the response in this case also depends on whether PIN can attach on every sides of
 230 the cell (apical/basal/lateral binding) or only on the lateral sides (lateral binding case), as attachment to the
 231 ‘useless’ apical and basal sides contribute to deplete PIN from the available pool. Overall, we see that only
 232 one case is compatible with the concave ‘sine-law’ shape observed experimentally: a limiting pool of PIN
 233 with lateral binding and $\mathcal{R} \gg 1$ (blue curve in Fig. 6 c).

234 In the following, we thus assume that PIN recycling occurs in the limited-pool regime ($\mathcal{P} \gg 1$), with
 235 lateral binding only. In this limit, and using expression of the surfaces given in Appendix B, the steady
 236 gravitropic response given by eqs. (12, 13, 14) can be written as:

$$\tilde{\Delta}^{\text{steady}}(\theta) = \frac{1}{2} \mathcal{A}(\mathcal{R} - 1) \begin{cases} \frac{W \tan \theta}{2H + 2(\mathcal{R} - 1)H_0} & \text{if } W \tan \theta < 2H_0 \\ \frac{\sqrt{2H_0 W \tan \theta}}{2H + (\mathcal{R} - 1)\sqrt{2H_0 W \tan \theta}} & \text{if } 2H_0 < W \tan \theta < H^2/(2H_0) \\ \frac{1}{\mathcal{R} + 1} & \text{else} \end{cases} \quad (15)$$

237 where the different conditions stand for cases where statoliths are totally absent left side, or totally covering
 238 the right side (see Fig. 7) and $\mathcal{A} = \frac{\alpha N_{\text{tot}} N}{\beta \int [ABCB]}$. Once the geometry of the cell and of the statoliths pile
 239 are fixed, the predicted gravitropic response depends on two dimensionless parameters: \mathcal{R} and \mathcal{A} . Fig.
 240 7 presents the experimental measurements of the ‘sine-law’ obtained by Chauvet et al. (2016) on wheat
 241 coleoptiles, together with the best fit of the (noisy) data using a least-square method. Reasonable agreement
 242 between theory and experiments is obtained with $\mathcal{R} \simeq 25$ and $\mathcal{A} \simeq 1.3$. It is interesting to note that within

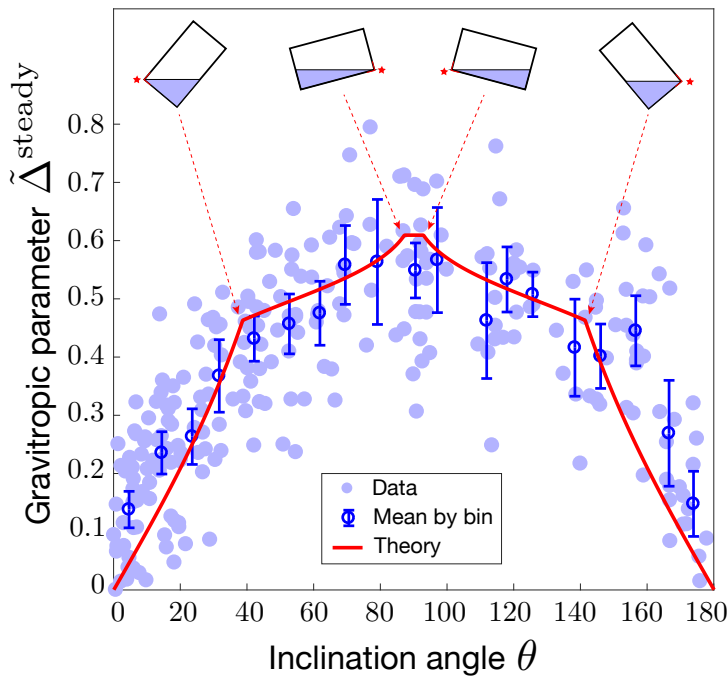


Figure 7. Modified sine-law $\tilde{\Delta}^{\text{steady}}$ as a function of the inclination angle θ . Comparison between the model prediction for $\mathcal{P} \ll 1$ (limiting pool) and l-binding (eq. (15) with $\mathcal{R} = 25$ and $\mathcal{A} = 1.3$, red line) and experiments on wheat coleoptiles (symbols, Chauvet et al. (2016)). Geometrical parameters used in the model for the statocyte are $H_0 = 4d$, $W = 10d$, $H = 25d$ where d stands for the diameter of a statolith. Error bars are the mean value of the data by binning the $[0,180]$ interval into 20 boxes.

243 our position-sensor framework, the predicted steady gravitropic response is not a simple ‘sine-law’, but
 244 rather a piece-wise curve with an overall concave shape. This law is also not universal and can be affected
 245 by several anatomical and physiological properties, such as the geometry of the cell H/W , the amount of
 246 statoliths H_0/W , or the molecular signaling machinery (embedded in the parameters \mathcal{R} and \mathcal{A}).

247
 248 **3.2 Transient gravitropic response: dose-response law**

249 The previous results deal with the steady gravitropic response obtained when the gravity stimulus (the
 250 angle of inclination θ) is permanent. We now turn to the study of the transient gravitropic response, i.e.,
 251 when the system has not yet reached the steady state. This situation typically corresponds to ‘dose-response’
 252 like experiments, in which the gravity stimulus is applied during a transient time ΔT only. Using such
 253 protocol on wheat coleoptiles, Chauvet et al. (2019) revealed the existence of an intrinsic ‘memory’ time
 254 τ_{memory} in the gravitropic response. For $\Delta T \gg \tau_{\text{memory}}$, the response was constant and equal to the steady
 255 response $\tilde{\Delta}^{\text{steady}}$. However, for $\Delta T \lesssim \tau_{\text{memory}}$, the response was smaller and became proportional to ΔT
 256 (Fig. 8). The memory time $\tau_{\text{memory}} \sim 15$ min identified in these experiments was longer than the sediment
 257 time of statoliths (~ 2 min) but shorter than the growth timescale (hours). It thus reflects a temporal process
 258 in the gravitropic signaling pathway that remains to be identified. We address below this question in the
 259 framework of the model.

260 The set of equations (5)-(7) give a complete description of the transient gravitropic response (we assume
 261 that sedimentation of statoliths is fast enough that the surfaces in (7) can be computed from their equilibrium
 262 values – see Appendix B). Two different typical times control the dynamics: τ_{aux} , describing the transport
 263 of auxin across the tissue of length $2R$, and τ_{PIN} , describing the dynamics of PIN at molecular scale. The

264 time scale associated to auxin transport τ_{aux} can be estimated using eq. (5) for a constant coefficient of
 265 diffusion \mathcal{D} and transport velocity v (i.e., PIN distribution). In this case, relaxation towards the stationary
 266 profile eq. (8) is exponential and occurs on a time scale set by the inverse of the shortest non-vanishing
 267 eigen-mode of equation (5):

$$\tau_{\text{aux}} = \frac{1}{\pi^2 + (\text{Pe}^2/4)} \times \frac{(2R)^2}{\mathcal{D}} \quad (16)$$

268 with $\text{Pe} = (2Rv)/\mathcal{D}$ Mohsen and Baluch (1983). Estimating the Peclet number from the steady gravitropic
 269 response ($\text{Pe} = 2\tilde{\Delta}^{\text{steady}} \approx 1$, see Fig. 7), and the auxin transport speed v from measurements of the speed
 270 of auxin pulses in plant tissues ($v \simeq 3\mu\text{ms}$, Goldsmith (1977); Rashotte et al. (2003)), gives $\tau_{\text{aux}} \simeq 30\text{s}$
 271 (we take $2R \sim 1\text{ mm}$). This is much shorter than the memory time $\tau_{\text{memory}} \sim 15\text{ min}$ evidenced in
 272 dose-response experiments, and even not larger than the statoliths sedimentation time. This suggests that
 273 the dynamics of the gravitropic response is controlled by τ_{PIN} , rather than by the auxin diffusion time τ_{aux} .

274 The time scale τ_{PIN} is set by the slowest characteristic time of the system Eq. (7) describing PIN dynamics.
 275 From the eigenvalues of this linear system, those two timescales are obtained, which are solutions of:

$$\begin{aligned} &\tau^{-2} - (k_{\text{off},0} + k_{\text{off},1} + [k_{\text{on},0}S_0 + k_{\text{on},1}S_1]/N_{\text{tot}})\tau^{-1} \\ &+ (k_{\text{off},0} + k_{\text{on},0}S_0/N_{\text{tot}})(k_{\text{off},1} + k_{\text{on},1}S_1/N_{\text{tot}}) - k_{\text{on},0}k_{\text{on},1}S_0S_1/N_{\text{tot}}^2 = 0. \end{aligned} \quad (17)$$

276 In the limiting pool case ($N_{\text{tot}}k_{\text{off},i}/k_{\text{on},i}S_i \ll 1$), the two solutions are:

$$\tau_1 = \frac{N_{\text{tot}}}{k_{\text{on},0}S_0 + k_{\text{on},1}S_1} \quad \text{and} \quad \tau_2 = \frac{k_{\text{on},0}S_0 + k_{\text{on},1}S_1}{k_{\text{off},0}k_{\text{on},1}S_1 + k_{\text{off},1}k_{\text{on},0}S_0}, \quad (18)$$

277 with $\tau_1 \ll \tau_2$. Therefore, the slowest time scale of the gravitropic signaling pathway, which sets τ_{memory} ,
 278 should be given by $\tau_{\text{PIN}} = \tau_2$. Note that when preferential attachment in region with statolith is achieved via
 279 a strongly increased attachment rate ($k_{\text{on},1} \gg k_{\text{on},0}$) and not by change of detachment rate ($k_{\text{off},0} \simeq k_{\text{off},1}$)
 280 we have $\tau_{\text{PIN}} = k_{\text{off}}^{-1}$. Conversely, if it is achieved by decreased detachment rate ($k_{\text{off},0} \gg k_{\text{off},1}$) and not by
 281 change of attachment rate ($k_{\text{on},0} \simeq k_{\text{on},1}$) we have $\tau_{\text{PIN}} = k_{\text{off},0}^{-1}(1 + S_1/S_0) \simeq k_{\text{off},0}^{-1}$. Remarkably, in this
 282 last case, the equilibration time of PIN is not controlled by the slowest rate of detachment ($k_{\text{off},1}$), but by
 283 the fastest one ($k_{\text{off},0}$), due to the limiting pool.

284 To check these predictions, we solve the model for a transient gravitropic stimulus that reproduces the
 285 protocol of Chauvet et al. (2019). The inclination θ is set to 45° for a transient time ΔT and then put back
 286 to zero, the gravitropic response being defined as the maximal auxin gradient reached during the dynamics:
 287 $\tilde{\Delta}^{\text{trans}} = \text{Max}[\frac{c_{\text{bottom}}(t) - c_{\text{top}}(t)}{2c_{\text{mean}}}]$. Fig. 8(a) compares the experimental data of Chauvet et al. (2019) with
 288 the prediction of the model for $\tau_{\text{aux}}/\tau_{\text{PIN}} \ll 1$, using the parameters \mathcal{R} and \mathcal{A} already fixed by the steady
 289 response (see Fig. 7). Good agreement is obtained using $\tau_{\text{PIN}} = 13\text{ min}$ as the only fitting parameter. This
 290 result shows that τ_{PIN} is playing the role of the memory time evidenced by the experiments of Chauvet
 291 et al. (2019). If $\Delta T \ll \tau_{\text{PIN}}$, PIN-transporters have not enough time to rearrange before the end of the
 292 stimulus, and the response is weak. Conversely if $\Delta T \gg \tau_{\text{PIN}}$, PIN have time to rearrange and reach their
 293 steady repartition before the end of the stimulus, and the response is maximal, similar to the one of a
 294 permanent stimulus.

295 We finish our analysis by investigating the full temporal dynamics of the gravitropic response after a
 296 sudden inclination $\theta = 50^\circ$. Fig. 8(b) presents the time evolution of the shoot curvature $\mathcal{C}(t)$ (or similarly
 297 $\theta_{\text{tip}}(t)$ for small curvatures) predicted by the model for $\tau_{\text{PIN}} = 13\text{ min}$ (blue curve), together with the

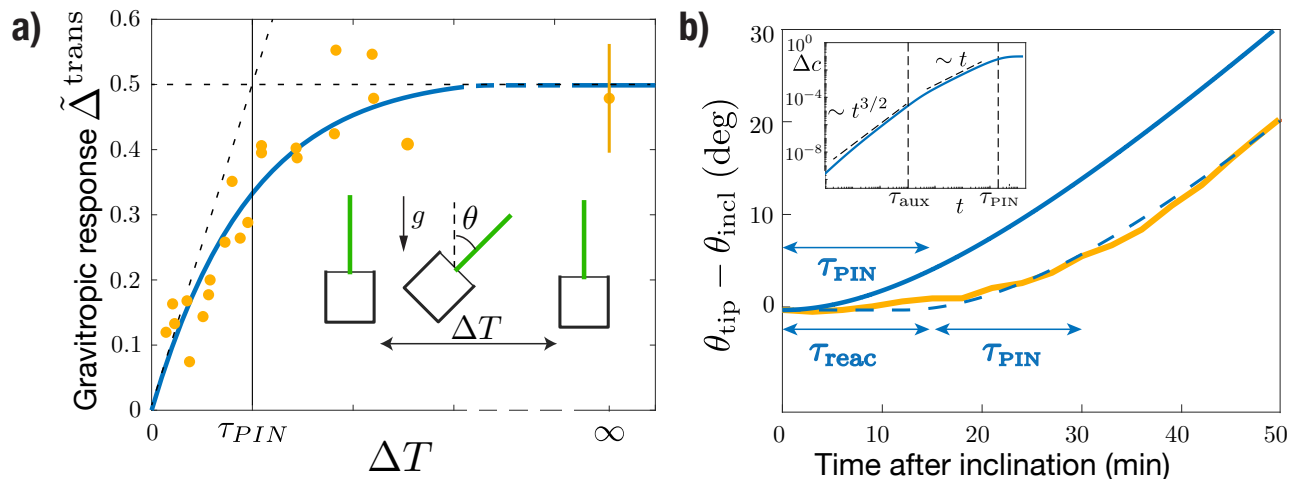


Figure 8. Gravitropic response to a transient inclination (dose-response like protocol). (a) Maximal gravitropic response reached during the dynamics as function of the inclination time ΔT for $\theta = 45^\circ$. The blue solid line is the model prediction using $\tau_{PIN} = 13$ min (τ_{aux}/τ_{PIN} and $\tau_1/\tau_{PIN} \ll 1$, other parameters are fixed as in Fig. 7). Symbols correspond to the aggregation results of (Chauvet et al., 2019) under $1g$ and $3g$. (b) Evolution of the tip angle after an inclination $\theta = 50^\circ$ predicted by the model with the same parameters (blue solid line) and in the experiments of Chauvet et al. (2016) (orange thick line). The predicted model must be shifted by a constant time $\tau_{reac} = 13$ min (thin red line) to match the experimental curve. Inset: early time behavior of the gravitropic response predicted by the model in log-log scale.

298 experimental data of Chauvet et al. (2016) (yellow curve). The time scale of the curvature change τ_{PIN} is
 299 well captured by the model. However, to match the experiments, the model has to be shifted in time by a
 300 constant time $\tau_{reac} \approx 13$ min. Such delay or reaction time of the gravitropic response after the stimulus
 301 was already noticed by Chauvet et al. (2019), but does not seem described by the model. Actually, a careful
 302 analysis of the temporal behavior of the model (assuming $\tau_1 \ll \tau_{aux} \ll \tau_{PIN} = \tau_2$) shows that the auxin
 303 gradient at early times increases as $\Delta c \sim t^{3/2}$ (so that $C \propto \int_0^t \Delta c dt \propto t^{5/2}$) as long as $t < \tau_{aux}$, before
 304 varying as $\Delta c \sim t$ for $\tau_{aux} < t < \tau_{PIN}$ (Inset of Fig. 8 b). These scaling laws are thus not compatible with
 305 a very flat initial response.

4 DISCUSSION

306 In this paper, we have derived a multi-scale model of plant gravitropism which links the different steps of
 307 the gravitropic signaling pathway: (i) the initial intracellular perception of gravity by statoliths, (ii) the
 308 transduction of this physical signal into a biochemical signal through the reorganization of PINs at the
 309 membrane of statocytes, (iii) the intercellular signal transmission via auxin transport and (iv) asymmetric
 310 organ growth. The main originality of the model lies in the mechanistic link we propose between the
 311 statoliths position and the dynamics of PIN, based on the recent position-sensor hypothesis (Pouliquen
 312 et al., 2017). This basic assumption coupled to auxin transport and growth in an idealized tissue made of a
 313 one-dimensional array of cells recovers several major features of the gravitropic response of plants.

314 4.1 A new interpretation of the sine-law of plant gravitropism

315 The first main result concerns the steady gravitropic response to a permanent gravity stimulus, $\tilde{\Delta}^{steady}(\theta)$.
 316 For many plants, this response takes the form of an inclination-dependent law with a sine-like shape, called
 317 for this reason the sine-law of plant gravitropism (Sachs, 1887; Larsen, 1969; Iino et al., 1996; Galland,
 318 2002; Dumais, 2013). This sine-law has long been interpreted in terms of a force sensor mechanism, for
 319 the projected weight of the statoliths on the lateral surface of the cell varies with the sine of the inclination

320 angle (Audus, 1969; Barlow, 1995). However, recent experiments showing that the response is independent
 321 of the gravity intensity have dismissed this force-sensing hypothesis, calling for a new interpretation of
 322 the sine law (Chauvet et al., 2016; Pouliquen et al., 2017). A key result of the model is that it predicts an
 323 inclination-dependent steady gravitropic response $\tilde{\Delta}^{\text{steady}}(\theta)$ without invoking a force-based mechanism.
 324 In the model, the initial gravitropic stimulus is the statoliths position at the cell membrane, not their weight.
 325 Since statoliths behave on long time like a liquid (Bérut et al., 2018), their position in steady state is a
 326 purely geometrical cue, which depends only on the cell inclination. As a result, the steady gravitropic
 327 response predicted by the model depends on the inclination but not on the gravity intensity, in agreement
 328 with the observations.

329 In the model, the actual shape of the gravitropic response $\tilde{\Delta}^{\text{steady}}(\theta)$ is never a pure sine law. It depends
 330 on several parameters, related either to geometric factors, such as the aspect ratios of the statocytes and
 331 of the sedimented statoliths pile, or to molecular processes: parameter \mathcal{R} , characterizing the intensity of
 332 coupling between statoliths position and PINs; parameter \mathcal{P} , characterizing the number of PINs available
 333 inside the cell; parameter \mathcal{A} , characterizing the ratio between the conductance of PIN carriers to the total
 334 conductance of auxin transporters. For elongated cells and shallow statoliths piles such as those of wheat
 335 coleoptile statocytes, the shape of the response tends to be sine-like only in the case of a strong coupling
 336 between the statoliths and PINs ($\mathcal{R} \gg 1$), and for a number of PINs conserved along the cell membrane
 337 (limiting pool regime, $\mathcal{P} \ll 1$). This latter assumption is common in models of auxin transport (Runions
 338 et al., 2014; Retzer et al., 2019), while the strong coupling assumption might be compatible with the large
 339 asymmetry in PINs localization observed upon gravity stimulation (Friml et al., 2002; Harrison and Masson,
 340 2008; Kleine-Vehn et al., 2010). Interestingly, although gravity is absent from the model, the gravitropic
 341 response depends on the amount of statoliths through the geometrical aspect ratio of the statoliths pile
 342 H_0/W . The model could thus account for previous experiments using starch-less and starch-excess mutants,
 343 which showed a modified gravitropic response when the number of statoliths is changed (Kiss et al., 1997;
 344 Vitha et al., 2007; Pouliquen et al., 2017). Finally, it is worth noting that the model assumes that the
 345 statoliths form a static pile at the bottom of the cell, while statoliths actually exhibit a dynamic and random
 346 agitation due to the interaction with the cytoskeleton (Sack et al., 1986; Saito et al., 2005; Nakamura et al.,
 347 2011; Bérut et al., 2018). We might expect this agitation to reduce the averaged contact time between the
 348 statoliths and the cell membrane, thereby decreasing the coupling between statoliths and PINs. It would be
 349 interesting to extend the model in order to incorporate such effect of agitation on the gravitropic response.
 350 The model could then be compared with the behavior of agravitropic mutants in *Arabidopsis thaliana*
 351 like *sgr9*, whose weaker response is likely associated to an abnormally strong agitation of the statoliths
 352 (Nakamura et al., 2011).

353 Overall, our model suggests that the classical sine-law of plant gravitropism might not be universal, as its
 354 shape and amplitude could depend on several anatomical and physiological parameters. Full measurements
 355 of the gravitropic response of plants over a wide range of inclination are scarce and mostly performed on
 356 shoot coleoptiles. It would be interesting to perform systematic measurements of the sine-law on other
 357 plant organs (root, stem), to see if the shape of the sine-law is affected by different statocyte geometries
 358 and tissue organization.

359 **4.2 The gravity-independent memory process in dose-response laws is likely** 360 **associated to PIN dynamics**

361 The second main result of our study concerns the gravitropic response to a transient gravity stimulus.
 362 For a sudden inclination applied at time $t = 0$, the model predicts that the response reaches the steady
 363 response $\tilde{\Delta}^{\text{steady}}(\theta)$ only after a time large compared to a ‘memory’ timescale τ_{memory} , corresponding

364 to the slowest timescale introduced in the model. Therefore, when a stimulus is applied only during a
365 transient time $\Delta T < \tau_{\text{memory}}$, a weaker gravitropic response is predicted, following a dose-response like
366 law. In the model, the memory time is not associated with the sediment time of the statoliths, which is
367 assumed much shorter than the other timescales of the gravitropic signaling pathway (a valid assumption
368 for a gravity intensity like Earth gravity). Our model is therefore compatible with the recent experiments of
369 Chauvet et al. (2019) performed on wheat coleoptiles, which shows a dose-like behavior of the gravitropic
370 response with a memory time τ_{memory} independent of gravity. It also provides the explicit origin of this
371 memory process, which was postulated in the model of Chauvet et al. (2019). Two different processes in the
372 model lead to the temporal filtration of the first signal associated with statoliths position: auxin transport
373 across the tissue and the dynamics of PIN turnover at the molecular scale. Our study suggests that the
374 limiting process is actually controlled by PIN dynamics ($\tau_{\text{memory}} = \tau_{\text{PIN}}$), auxin transport being too fast
375 to account for the memory time measured experimentally ($\sim 10\text{-}20$ min). Interestingly, visualization of the
376 PIN3 auxin efflux carrier in root columella cells after a sudden change in the gravity vector indicates a time
377 scale of about 10 min for complete relocation (Friml et al., 2002), a duration very close to the memory time
378 measured by (Chauvet et al., 2019). Although our model successfully captures the existence and origin
379 of a gravity-independent memory process in the signaling pathway, it is not able to describe the delay
380 time $\tau_{\text{reaction}} \sim 10$ min observed between the application of the stimulus and the first gravitropic response
381 (Chauvet et al., 2019). We might rationalize it as the time needed to reorganize the cytoskeleton implied in
382 the transport of PIN carriers, the time needed by a PIN to go from the pool towards the plasma membrane,
383 or the time of incorporation of a PIN into the membrane. It is worth noting that a similar timescale of about
384 10 min was identified in the gravity-sensing columella cells for the internalization of PIN3 from the plasma
385 membrane into vesicles (Kleine-Vehn et al., 2010). Further experiments combining a transient stimulus
386 with pharmacological and genetic approaches would be needed to confirm the key role of the PIN turnover
387 timescale in the gravitropic response.

388 4.3 Back to the statoliths/PIN coupling assumption

389 We conclude by discussing the possible origin of the coupling between statoliths and PINs, which is
390 at the core of our model. Although the respective roles of statoliths and PIN auxin transporters in plant
391 gravitropism are now well established, the link between the two is still not clear (see Nakamura et al. (2019)
392 for a recent review of the possible molecular actors involved). In our model, we have used a very general
393 hypothesis for this coupling based on the recent finding that the relevant gravitropic stimulus is the statoliths
394 position inside the gravisensing cells (Chauvet et al., 2016; Pouliquen et al., 2017; Bérut et al., 2018). We
395 have postulated that statoliths in contact with the cell membrane bias the exocytosis and endocytosis rate of
396 PIN recycling, therefore inducing an asymmetry of PIN distribution when statoliths reposition in response
397 to plant inclination. Our results suggest that this interaction between PINs and statoliths is strong, as large
398 values of the parameter \mathcal{R} are needed to match the experimental gravitropic response. This interaction
399 between statoliths and PINs could involve a complex molecular pathway that remains to be unveiled
400 (Strohm et al., 2014). However, more direct mechanisms of interaction could occur. For example, statoliths
401 could modify PIN vesicle-mediated transportation to the membrane by modifying the architecture of the
402 actin cytoskeleton. Another possibility would be that internalization of PINs from the membrane is reduced
403 by the presence of statoliths, for example by simple steric effects. Indeed, direct visualizations reveal a
404 length scale of $\sim 1 \mu\text{m}$ for the endosome formation, which is not far from statolith size (Kleine-Vehn et al.,
405 2010). Interestingly, such direct interaction of statoliths and the cytoskeleton machinery was put forward as
406 an explanation of gravitropism in rhizoids and protonemata like the single-cell alga *Chara* (Sievers et al.,
407 1996). A last possibility could be that PINs cluster in regions where there is no statolith, while they do not
408 cluster when statoliths are present. Indeed, for a conserved number of PIN proteins, clustering reduces

409 the efflux efficiency, as this diffusion process scales not linearly but as the square-root of the number of
 410 carriers Bénichou and Voituriez (2014); Valet et al. (2019). Such a clustering has been highlighted by
 411 Kleine-Vehn et al. (2011), but, to our knowledge, no comparison has been done between regions with and
 412 without statoliths. Further studies are thus needed to discriminate between these molecular mechanisms.

CONFLICT OF INTEREST STATEMENT

413 The authors declare that the research was conducted in the absence of any commercial or financial
 414 relationships that could be construed as a potential conflict of interest.

AUTHOR CONTRIBUTIONS

415 N.L., O.P., and Y.F. designed research. N.L. built and analyzed the model with inputs from O.P. and Y.F.
 416 N.L., O.P., and Y.F. wrote the paper..

FUNDING

417 This work was supported by the European Research Council (ERC) under the European Union's Horizon
 418 2020 research and innovation programme (grant agreement N°647384) and by the French National Agency
 419 (ANR) under the program Blanc Grap2 (ANR-13-BSV5-0005-01).

ACKNOWLEDGMENTS

420 The authors would like to thank Valérie Legué and Bruno Moulia for the many stimulating discussions we
 421 have continually had on this subject.

APPENDIX A: CASE OF STATOLITHS ONLY PRESENT ON A RING

422 Let be a central region between l and $2R - l$ with no statolith (and constant efflux rate P_0). We can redo the
 423 calculation leading to (4) in this geometry. Clearly, equations will be similar in each region, with $v = 0$ in
 424 the central one. We have to take care to the continuity of the flux at the junction of each regions. We can show
 425 that $J(l) = (P + \delta P)c(l^-) - P_0c(l^+)$ and $J(2R - l) = P_0c((2R - l)^-) - Pc((2R - l)^+)$. At steady state, we
 426 thus get a jump of auxin concentration: $c(l^+) = (P + \delta P)/P_0 c(l^-)$ and $c((2R - l)^+) = P_0/P c((2R - l)^-)$.
 427 In the limit of small Peclet number, we thus get $\Delta c/c = (P_0/P)(vl/\mathcal{D})$.

APPENDIX B: EXPRESSION OF THE GEOMETRIC PARAMETERS AS A FUNCTION OF θ

We give here the value of the surfaces $S_i^{r,l}(\theta)$ that are necessary to compute the Peclet number as a function of the angle (see Eq. (15)). As statoliths are solid, the shaded area in 3 is conserved and is thus equal to H_0W . We note $\theta_1 = \arctan 2H_0/W$ the angle for which the horizontal level meets the lower left corner, and $\theta_2 = \arctan H^2/(2H_0W)$ the one for which it meets the upper right one (we assume $H_0 < H/2$). Elementary geometry calculations give:

$$S_0^l = \begin{cases} H - H_0 + \frac{W \tan \theta}{2} & \text{if } \theta < \theta_1 \\ H & \text{else} \end{cases} \quad (19)$$

$$S_1^l = \begin{cases} H_0 - \frac{W \tan \theta}{2} & \text{if } \theta < \theta_1 \\ 0 & \text{else} \end{cases} \quad (20)$$

$$S_0^r = \begin{cases} H - H_0 - \frac{W \tan \theta}{2} & \text{if } \theta < \theta_1 \\ H - \sqrt{2H_0W \tan \theta} & \text{if } \theta_1 < \theta < \theta_2 \\ 0 & \text{else} \end{cases} \quad (21)$$

$$S_1^r = \begin{cases} H_0 + \frac{W \tan \theta}{2} & \text{if } \theta < \theta_1 \\ \sqrt{2H_0W \tan \theta} & \text{if } \theta_1 < \theta < \theta_2 \\ H & \text{else} \end{cases} \quad (22)$$

In the case of apical binding, this leads to

$$S_0 = \begin{cases} 2(H - H_0) & \text{if } \theta < \theta_1 \\ 2H - \sqrt{2H_0W \tan \theta} & \text{if } \theta_1 < \theta < \theta_2 \\ H & \text{else} \end{cases} \quad (23)$$

$$S_1 = \begin{cases} 2H_0 & \text{if } \theta < \theta_1 \\ \sqrt{2H_0W \tan \theta} & \text{if } \theta_1 < \theta < \theta_2 \\ H & \text{else} \end{cases} \quad (24)$$

428 In the case of apical/basal/lateral binding, the expressions for the total surfaces are slightly modified due to
429 attachment at apical and basal side.

REFERENCES

- 430 Audus, L. (1969). Geotropism. In *The physiology of plant growth and development* (McGraw-Hill,
431 London). 203–241
- 432 Band, L. R., Wells, D. M., Larrieu, A., Sun, J., Middleton, A. M., French, A. P., et al. (2012). Root
433 gravitropism is regulated by a transient lateral auxin gradient controlled by a tipping-point mechanism.
434 *Proceedings of the National Academy of Sciences* 109, 4668
- 435 Barlow, P. W. (1995). Gravity perception in plants: a multiplicity of systems derived by evolution? *Plant,*
436 *Cell & Environment* 18, 951–962
- 437 Bastien, R., Bohr, T., Moulia, B., and Douady, S. (2013). Unifying model of shoot gravitropism reveals
438 proprioception as a central feature of posture control in plants. *Proceedings of the National Academy of*
439 *Sciences* 110, 755–760
- 440 Bastien, R., Douady, S., and Moulia, B. (2014). A unifying modeling of plant shoot gravitropism with an
441 explicit account of the effects of growth. *Frontiers in plant science* 5, 136
- 442 Bénichou, O. and Voituriez, R. (2014). From first-passage times of random walks in confinement to
443 geometry-controlled kinetics. *Physics Reports* 539, 225–284
- 444 Bérut, A., Chauvet, H., Legué, V., Moulia, B., Pouliquen, O., and Forterre, Y. (2018). Gravisensors in plant
445 cells behave like an active granular liquid. *Proceedings of the National Academy of Sciences* 115, 5123
- 446 Chauvet, H., Moulia, B., Legué, V., Forterre, Y., and Pouliquen, O. (2019). Revealing the hierarchy of
447 processes and time-scales that control the tropic response of shoots to gravi-stimulations. *Journal of*
448 *Experimental Botany* 70, 1955–1967

- 449 Chauvet, H., Pouliquen, O., Forterre, Y., Legué, V., and Moullia, B. (2016). Inclination not force is sensed
450 by plants during shoot gravitropism. *Scientific reports* 6, 35431–35431
- 451 Chelakkot, R. and Mahadevan, L. (2017). On the growth and form of shoots. *Journal of The Royal Society*
452 *Interface* 14, 20170001
- 453 Dumais, J. (2013). Beyond the sine law of plant gravitropism. *Proceedings of the National Academy of*
454 *Sciences* 110, 391–392
- 455 Dyson, R. J., Vizcay-Barrena, G., Band, L. R., Fernandes, A. N., French, A. P., Fozard, J. A., et al. (2014).
456 Mechanical modelling quantifies the functional importance of outer tissue layers during root elongation
457 and bending. *New Phytologist* 202, 1212–1222
- 458 Fendrych, M., Akhmanova, M., Merrin, J., Glanc, M., Hagihara, S., Takahashi, K., et al. (2018). Rapid and
459 reversible root growth inhibition by tir1 auxin signalling. *Nature plants* 4, 453–459
- 460 Friml, J., Wiśniewska, J., Benková, E., Mendgen, K., and Palme, K. (2002). Lateral relocation of auxin
461 efflux regulator pin3 mediates tropism in arabidopsis. *Nature* 415, 806–809
- 462 Galland, P. (2002). Tropisms of avena coleoptiles: sine law for gravitropism, exponential law for
463 photogravitropic equilibrium. *Planta* 215, 779–784
- 464 Galston, A. W. and Hand, M. E. (1949). Studies on the physiology of light action; auxin and the light
465 inhibition of growth. *Am J Bot* 36, 85–94
- 466 Goldsmith, M. H. M. (1977). The polar transport of auxin. *Annual Review of Plant Physiology* 28, 439–478
- 467 Grieneisen, V. A., Scheres, B., Hogeweg, P., and M Marée, A. F. (2012). Morphogengineering roots:
468 comparing mechanisms of morphogen gradient formation. *BMC Systems Biology* 6, 37
- 469 Harrison, B. R. and Masson, P. H. (2008). Arl2, arg1 and pin3 define a gravity signal transduction pathway
470 in root statocytes. *The Plant Journal* 53, 380–392
- 471 Hopkins, W. G. and Hüner, N. P. (2009). *Introduction to Plant Physiology 4th ed*
- 472 Iino, M., Tarui, Y., and Uematsu, C. (1996). Gravitropism of maize and rice coleoptiles: dependence on the
473 stimulation angle. *Plant, cell & environment* 19, 1160–1168
- 474 Kiss, J. Z., Guisinger, M. M., Miller, A. J., and Stackhouse, K. S. (1997). Reduced gravitropism in
475 hypocotyls of starch-deficient mutants of arabidopsis. *Plant and Cell Physiology* 38, 518–525
- 476 Kleine-Vehn, J., Ding, Z., Jones, A. R., Tasaka, M., Morita, M. T., and Friml, J. (2010). Gravity-induced
477 pin transcytosis for polarization of auxin fluxes in gravity-sensing root cells. *Proceedings of the National*
478 *Academy of Sciences* 107, 22344–22349
- 479 Kleine-Vehn, J. and Friml, J. (2008). Polar targeting and endocytic recycling in auxin-dependent plant
480 development. *Annual Review of Cell and Developmental Biology* 24, 447–473
- 481 Kleine-Vehn, J., Wabnik, K., Martinière, A., Łangowski, Ł., Willig, K., Naramoto, S., et al. (2011).
482 Recycling, clustering, and endocytosis jointly maintain pin auxin carrier polarity at the plasma membrane.
483 *Molecular systems biology* 7, 540–540
- 484 Kramer, E. M., Frazer, N. L., and Baskin, T. I. (2007). Measurement of diffusion within the cell wall in
485 living roots of arabidopsis thaliana. *Journal of experimental botany* 58, 3005–3015
- 486 Krecek, P., Skupa, P., Libus, J., Naramoto, S., Tejos, R., Friml, J., et al. (2009). The pin-formed (pin)
487 protein family of auxin transporters. *Genome biology* 10, 249–249
- 488 Kutschera, U. and Niklas, K. (2007). The epidermal-growth-control theory of stem elongation: an old and
489 a new perspective. *Journal of plant physiology* 164, 1395–1409
- 490 Larsen, P. (1969). The optimum angle of geotropic stimulation and its relation to the starch statolith
491 hypothesis. *Physiologia Plantarum* 22, 469–488
- 492 Meroz, Y., Bastien, R., and Mahadevan, L. (2019). Spatio-temporal integration in plant tropisms. *Journal*
493 *of the Royal Society Interface* 16, 20190038

- 494 Mohsen, M. F. N. and Baluch, M. H. (1983). An analytical solution of the diffusion-convection equation
495 over a finite domain. *Applied mathematical modelling* 7, 285–287
- 496 Morita, M. T. (2010). Directional gravity sensing in gravitropism. *Annual review of plant biology* 61,
497 705–720
- 498 Moulia, B. and Fournier, M. (2009). The power and control of gravitropic movements in plants: a
499 biomechanical and systems biology view. *Journal of experimental botany* 60, 461–486
- 500 Nakamura, M., Nishimura, T., and Morita, M. T. (2019). Gravity sensing and signal conversion in plant
501 gravitropism. *Journal of experimental botany* 70, 3495–3506
- 502 Nakamura, M., Toyota, M., Tasaka, M., and Morita, M. T. (2011). An arabidopsis e3 ligase, shoot
503 gravitropism9, modulates the interaction between statoliths and f-actin in gravity sensing. *The Plant*
504 *Cell* 23, 1830–1848
- 505 Pouliquen, O., Forterre, Y., Bérut, A., Chauvet, H., Bizet, F., Legue, V., et al. (2017). A new scenario for
506 gravity detection in plants: the position sensor hypothesis. *Physical Biology* 14, 035005
- 507 Rashotte, A. M., Poupard, J., Waddell, C. S., and Muday, G. K. (2003). Transport of the two natural auxins,
508 indole-3-butyric acid and indole-3-acetic acid, in arabidopsis. *Plant Physiology* 133, 761
- 509 Retzer, K., Akhmanova, M., Konstantinova, N., Malínská, K., Leitner, J., Petrášek, J., et al. (2019).
510 Brassinosteroid signaling delimits root gravitropism via sorting of the arabidopsis pin2 auxin transporter.
511 *Nature communications* 10, 1–15
- 512 Runions, A., Smith, R. S., and Prusinkiewicz, P. (2014). Computational models of auxin-driven
513 development. In *Auxin and its role in plant development* (Springer). 315–357
- 514 Sachs, J. (1887). *Lectures on the Physiology of Plants* (Clarendon Press)
- 515 Sack, F. D., Suyemoto, M. M., and Leopold, A. C. (1986). Amyloplast sedimentation and organelle
516 saltation in living corn columella cells. *American journal of botany* 73, 1692–1698
- 517 Saito, C., Morita, M. T., Kato, T., and Tasaka, M. (2005). Amyloplasts and vacuolar membrane dynamics
518 in the living graviperceptive cell of the arabidopsis inflorescence stem. *The Plant Cell* 17, 548–558
- 519 Sievers, A., Buchen, B., and Hodick, D. (1996). Gravity sensing in tip-growing cells. *Trends in plant*
520 *science* 1, 249–250
- 521 Silk, W. K. (1984). Quantitative descriptions of development. *Ann. Rev. Plant Physiol.* 35, 479–518
- 522 Strohm, A. K., Barrett-Wilt, G. A., and Masson, P. H. (2014). A functional toc complex contributes to
523 gravity signal transduction in arabidopsis. *Frontiers in plant science* 5, 148
- 524 Toyota, M. and Gilroy, S. (2013). Gravitropism and mechanical signaling in plants. *American journal of*
525 *botany* 100, 111–125
- 526 Valet, M., Pontani, L.-L., Voituriez, R., Wandersman, E., and Prevost, A. M. (2019). Diffusion through
527 nanopores in connected lipid bilayer networks. *Phys. Rev. Lett.* 123, 088101
- 528 Vitha, S., Yang, M., Sack, F. D., and Kiss, J. Z. (2007). Gravitropism in the starch excess mutant of
529 arabidopsis thaliana. *American journal of botany* 94, 590–598
- 530 Zažímalová, E., Murphy, A. S., Yang, H., Hoyerová, K., and Hošek, P. (2010). Auxin transporters why so
531 many? *Cold Spring Harbor perspectives in biology* 2, a001552